Instability theory of swirling flows with suction

Basile GALLET, supervised by C.Doering and E.Spiegel

August 24, 2007

1 Introduction

Accretion disks radiate a tremendous amount of energy. In these systems the only source of energy is gravitational energy. Turbulence in the disk converts this gravitational energy into heat and finally radiation. During this process the angular momentum of the fluid is carried out by turbulent transport, which allows accretion of the fluid onto the central object. Without turbulence the angular momentum would not be carried out efficientely enough and the accretion rate would be extremely low. The velocity profile of an accretion disk is considered to be mostly Keplerian, and the accretion rate is quite low, which means that the motion of the fluid inside the disk is almost circular. However, circular Keplerian flows are known to be linearly stable and one may wonder how turbulence is generated in such a system.

If the magnetic field inside the disk is high enough, it has been shown that the magnetorotational instability (MRI) can destabilize the flow and produce turbulence [3]. This provides at least one mechanism to drive turbulence in accretion disks. However, it has been shown that the MRI may be suppressed if the magnetic Prandtl number (ratio of the viscosity over the magnetic viscosity) is not high enough. In cold proptoplanetary nebulas for instance, the ionization is too low and one has to find another way to destabilize the flow than the MRI.

This is one of our main motivations to study the combined effects of both rotation and accretion on a very simple flow : the Taylor-Couette flow with inward suction. Although the astrophysical relevance of such a flow as a model of an accretion disk is quite limited, it can be used to show that taking into account both accretion and rotation leads to very different stability propreties of the flow than considering only rotation (circular flows) or only accretion (accretion onto a central object with a spherical symmetry). Both the energy stability and the linear stability of the flow are discussed in this report.

In section 2 we describe the Taylor-Couette flow with suction. The energy stability technique is described in section 3. Some rigorous bounds on the energy stability limit of the flow are derived in section 4, and the actual energy stability limit is computed numerically in section 5. Finding bounds on the energy dissipation of this flow appears to be very challenging. This is discussed in section 6. Finally the linear stability of the problem is studied in section 7.

2 Formulation of the problem

2.1 Geometry of the problem and boundary conditions

We study the incompressible motion of a Newtonian fluid between two concentric porous cylinders. In the configuration we focus on, the inner cylinder is maintained in a static position while the outer cylinder is rotating with constant angular velocity Ω. Let us write R_1 and R_2 the radii of the inner and outer cylinders and use cylindrical coordinates (r, θ, z). We assume no slip boundary conditions : the azimuthal and vertical components of the velocity field vanish at the two cylinders.

To this classical Taylor-Couette flow is added a radial inward suction : the fluid is injected through the outer cylinder with a flux Φ (volume of fluid injected per unit time and per unit height of cylinder) and sucked at the inner cylinder. Incompressibility imposes the conservation of the radial flux of fluid so that the fluid is removed at $R1$ with the same flux Φ. We consider the simplest problem in which the fluid is uniformly injected at $R2$ and removed at $R1$, which means that Φ is independant of both time and θ. If the velocity field is designated as $\overrightarrow{u} = u\overrightarrow{e_r} + v\overrightarrow{e_\theta} + w\overrightarrow{e_z}$, the boundary conditions are :

$$\overrightarrow{u}(R_1, \theta, z) = -\frac{\Phi}{2\pi R_1}\overrightarrow{e_r} \quad (1)$$

$$\overrightarrow{u}(R_2, \theta, z) = -\frac{\Phi}{2\pi R_2}\overrightarrow{e_r} + R_2\Omega\overrightarrow{e_\theta} \quad (2)$$

The incompressibility constraint $\overrightarrow{\nabla}.\overrightarrow{u} = 0$ adds two other boundary conditions :

$$u_r(R_1) = 0 \text{ and } u_r(R_2) = 0 \quad (3)$$

where the subscript r designate a derivative with respect to r. We assume periodic boundary conditions in the z direction with a period L_z.

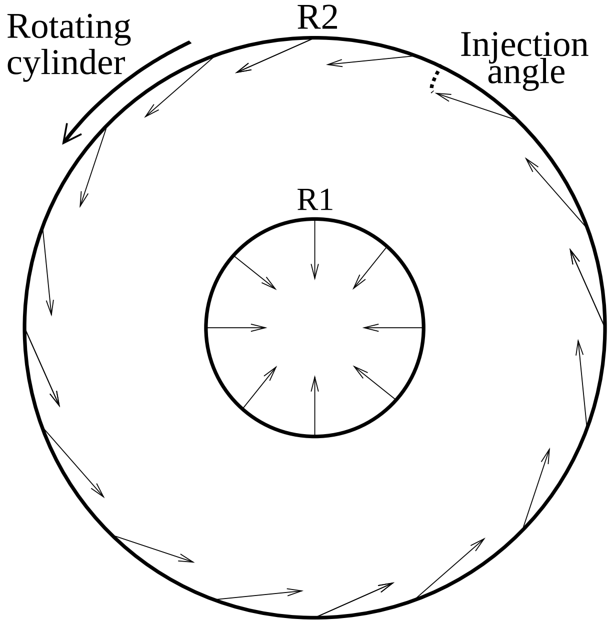

Figure 1: Schematic of the boundary conditions. The outer cylinder is rotating with an angular velocity Ω and the fluid is injected at the outer boundary with an entry angle Θ

2.2 Dimensionless numbers

The problem we are studying involves the 5 parameters : the two radii R_1 and R_2, the angular velocity of the outer cylinder Ω, the flux of injection Φ, and the viscosity of the fluid ν. These parameters can be expressed with one unit of time and one unit of length. We thus have in this problem $5 - 2 = 3$ dimensionless numbers in terms of which the physical results can be expressed :

- The geometrical factor $\eta = \frac{R_1}{R_2}$. When η goes to one we reach the narrow gap limit where $(R_2 - R_1) << R_1$. We expect to find results similar to the slab geometry (plane Couette flow with suction) in this limit. On the other hand, when η goes to zero, the outer radius R_2 goes to infinity if the inner radius remains constant. In this limit we expect to see some strong effects of the rotation on the stability of the flow, such as centrifugal effects.

- The injection angle at the outer cylinder, which we designate as Θ. This angle is linked to the radial and azimuthal components of the velocity field at the outer boundary :

$$tan(\Theta) = \frac{|U(R_2)|}{V(R_2)} = \frac{\Phi}{2\pi R_2^2 \Omega}$$

  If $tan(\Theta) = 0$ there is no suction and we recover the classical Taylor-Couette problem. When $tan(\Theta)$ goes to infinity we reach the limit in which there is mostly suction and almost no azimuthal velocity.

- The azimuthal Reynolds number :

$$Re = \frac{R_2 \Omega (R_2 - R_1)}{\nu}$$

  We choose this definition of the Reynolds number so that it matches the definition of the Reynolds number for the plane Couette flow when η goes to one.

Although only 3 dimensionless numbers are required to describe the physics of the system, it is useful to introduce also the radial Reynolds number $\alpha = \frac{\Phi}{2\pi\nu}$ to make the equations more compact. This number is linked to Re, η and $\tan(\Theta)$ by the relation :

$$\alpha = \frac{Re \tan(\Theta)}{1-\eta} \tag{4}$$

2.3 Laminar solution

The steady laminar solution of the problem $\overrightarrow{V_l} = (U(r), V(r), 0)$ is derived from the Navier-Stokes equations, together with the incompressibility condition $\overrightarrow{\nabla}.\overrightarrow{V_l} = 0$. The latter yields :

$$\begin{aligned} \frac{1}{r}(rU)_r &= 0 \\ U(r) = -\frac{\Phi}{2\pi r} & \end{aligned}$$

The azimuthal component of the Navier-Stokes equation is then :

$$\nu V_{rr} + \frac{V_r}{r}(\nu + \Psi) + \frac{V}{r^2}(\Psi - \nu) = 0$$

with $\Psi = \frac{\Phi}{2\pi}$. One can look for solutions of this equation in the form $V(r) = Ar^p$. We find 2 acceptable values for p :

$$p = -1 \text{ or } p = 1 - \alpha$$

The solution for V which matches the boundary conditions is then :

$$V = Ar^{1-\alpha} + \frac{B}{r} \text{ with } \left\{ \begin{array}{l} A = \frac{-R_2^2 \Omega}{R_1^{2-\alpha} - R_2^{2-\alpha}} \\ B = \frac{R_1^{2-\alpha} R_2^2}{R_1^{2-\alpha} - R_2^{2-\alpha}} \Omega \end{array} \right.$$

This azimuthal velocity profile is represented in figure 2 for different values of α and η.

When α goes to zero we recover the classical velocity field of the Taylor-Couette flow (with a steady inner cylinder), which is independant of the viscosity ν. The azimuthal velocity monotonously increases when r goes from R_1 to R_2.

However, for nonzero values of the entry angle $\tan(\Theta)$ and large values of the Reynolds number ($Re \tan(\Theta) >> 1$), going outward from the inner cylinder the azimuthal velocity rapidly increases in a boundary layer of thickness δ near the inner cylinder and then decreases from $R_1 + \delta$ to R_2. The azimuthal velocity profile has a maximum for $r = R_1 + \delta$:

$$V_r(R_1 + \delta) = 0 \Leftrightarrow R_1 + \delta = \left(\frac{B}{A(1-\alpha)}\right)^{\frac{1}{2-\alpha}} = \frac{R_1}{(1-\alpha)^{\frac{1}{2-\alpha}}}$$

For large values of α, the boundary layer is very thin and :

$$\frac{\delta}{R_1} = (\alpha - 1)^{\frac{1}{\alpha-2}} - 1 \simeq \frac{ln(\alpha)}{\alpha}$$

The physical origin of this non monotonous velocity profile is easy to understand : at high Reynolds number, the motion of the fluid is nearly inviscid. A fluid element injected at the outer boundary with the azimuthal velocity $R_2\Omega$ will spiral towards the center. It has to conserve its azimuthal angular momentum $rV(r)$ during this quasi-inviscid motion :

$$rV(r) = constant \Rightarrow V(r) = \frac{R_2^2\Omega}{r}$$

The azimuthal velocity of the fluid element increases during this inward movement, but it has to vanish at the inner boundary. The role of the viscous boundary layer is to dissipate the angular momentum of the incoming fluid so that the azimuthal velocity goes from $V_{max} \simeq \frac{R_2^2\Omega}{R_1} = \frac{R_2\Omega}{\eta}$ to zero at the inner cylinder. The fact that the azimuthal velocity profile has a high maximum is strongly linked to the cylindrical geometry of the problem, and this effect disappears in the plane limit $\eta \to 1$ since $\frac{V_{max}}{R_2\Omega} = \frac{1}{\eta}$.

One should notice that the asymptotic velocity profile at $Re \to \infty$ is dramatically modified from $\tan(\Theta) = 0$ to $\tan(\Theta) \neq 0$: if $\tan(\Theta) = 0$ the azimuthal velocity profile is the classical Taylor-Couette profile which is independant of the Reynolds number. However, if $\tan(\Theta) \neq 0$ the azimuthal velocity profile goes like $\frac{1}{r}$ everywhere inside the gap and the boundary layer becomes infinetely thin in the limit $Re \to \infty$. This shows that even if the accretion rate is very low, one cannot neglect it and study the problem with rotation only. Mathematically this is due to the fact that the limits $Re \to \infty$ and $\tan(\Theta) \to 0$ do not commute.

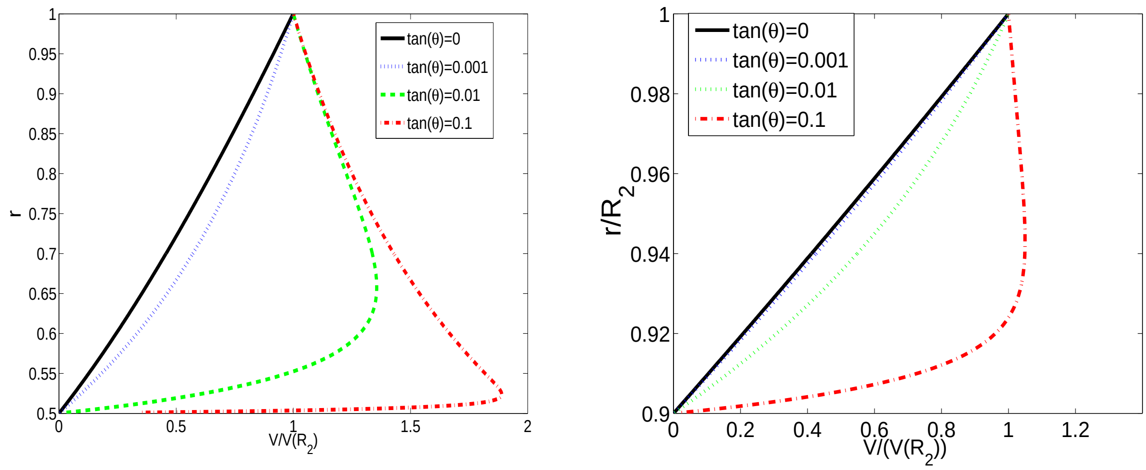

Figure 2: Azimuthal velocity profiles for different values of the entry angle. (Left : $\eta = 0.5$, right : $\eta = 0.9$)

3 Energy stability of the laminar solution

We study in this section the energy stability of the flow, a very strong form of stability in a sense which will be described precisely in paragraph 3.2. The energy stability technique provides sufficient conditions for a flow to be stable, but one should keep in mind that if a flow is not energy stable it can still be stable.

3.1 Decomposition of the velocity field

The starting point of this technique is to decompose the velocity field $\overrightarrow{u}$ into a steady background flow $\overrightarrow{V}$ and a time dependant field $\overrightarrow{v}$. We require both the background flow and the fluctuating field to be divergence free :

$$\overrightarrow{u}(\overrightarrow{r},t) = \overrightarrow{V}(\overrightarrow{r}) + \overrightarrow{v}(\overrightarrow{r},t) \text{ with } \left\{ \begin{array}{l} \overrightarrow{\nabla}.\overrightarrow{V} = 0 \\ \overrightarrow{\nabla}.\overrightarrow{v} = 0 \end{array} \right.$$

Moreover, the background flow has to verify the boundary conditions on $\overrightarrow{u}$ as they were specified in equations 1 and 2 , whereas the fluctuation field verifies the homogeneous boundary conditions $\overrightarrow{v} = \overrightarrow{0}$ at the two cylinders. Finally, both $\overrightarrow{V}$ and $\overrightarrow{v}$ are periodic in z with the same period L_z. We can introduce the decomposition of $\overrightarrow{u}$ into the Navier-Stokes equation to find :

$$\overrightarrow{v}_t + (\overrightarrow{v}.\overrightarrow{\nabla})\overrightarrow{v} + (\overrightarrow{V}.\overrightarrow{\nabla})\overrightarrow{v} + (\overrightarrow{v}.\overrightarrow{\nabla})\overrightarrow{V} + (\overrightarrow{V}.\overrightarrow{\nabla})\overrightarrow{V} + \overrightarrow{\nabla}(p) \quad = \quad \nu\Delta\overrightarrow{v} + \nu\Delta\overrightarrow{V} \tag{5}$$

To study the kinetic energy of the fluctuation field we need to take the dot product of this equation with $\overrightarrow{v}$ and integrate over one cell, i.e. over the domain $\tau = [R_1, R_2] \times [0, 2\pi] \times [0, L_z]$. Let us write $d\tau$ the volume element in this domain and define the standard N_2 norm as :

$$||\overrightarrow{f}||^2 = \int_\tau |\overrightarrow{f}|^2 d\tau$$

Then we perform a few integration by parts using the homogeneous boundary condition on $\overrightarrow{v}$ to find :

$$d_t\left(\frac{||\overrightarrow{v}||^2}{2}\right) + \int_\tau \overrightarrow{v}.[(\overrightarrow{V}.\overrightarrow{\nabla})\overrightarrow{V} - \nu\Delta\overrightarrow{V}]d\tau \quad = \quad -\int_\tau \nu|\overrightarrow{\nabla}\overrightarrow{v}|^2 + \overrightarrow{v}.(\overrightarrow{\nabla}\overrightarrow{V}).\overrightarrow{v}\,d\tau \tag{6}$$

3.2 Absolute stability

To study the energy stability of the laminar solution we let the background flow be this laminar solution $\overrightarrow{V_l}$. This makes the integral on the left hand side of equation 6 to vanish and leads to :

$$\left\{ \begin{array}{l} d_t\left(\frac{||\overrightarrow{v}||^2}{2}\right) = -\mathcal{H}\{\overrightarrow{v}\} \\ \text{with } \mathcal{H}\{\overrightarrow{v}\} = \int_\tau \nu|\overrightarrow{\nabla}\overrightarrow{v}|^2 + \overrightarrow{v}.(\overrightarrow{\nabla}\overrightarrow{V_l}).\overrightarrow{v}\,d\tau \end{array} \right.$$

$\mathcal{H}\{\overrightarrow{v}\}$ is a quadratic form in $\overrightarrow{v}$. If this quadratic form is strictly positive the kinetic energy of the perturbation $\overrightarrow{v}$ is a decreasing function of time. Moreover, we can prove thanks to Gronwall's inequality that it will decay at least like an exponential. We should emphasize the fact that we have not made any assumption on the size of the perturbation (as in linear theory for instance where the perturbation has to be infinitesimal), which means that any divergence-free perturbation of arbitrary amplitude which matches the homogeneous boundary conditions will be damped out : a flow for which $\mathcal{H}$ is a positive quadratic form has a very strong form of stability which is called energy stability or absolute stability.

Let us define the function $\mu(Re, \tan(\Theta))$ as :

$$\mu(Re, \tan(\Theta)) = \inf \frac{\mathcal{H}\{\overrightarrow{v}\}}{||\overrightarrow{v}||^2} \tag{7}$$

the infimum being taken over every divergence-free vector field satisfying the homogeneous boundary conditions. The absolute stability is achieved in the region of the $(Re, \tan(\Theta))$ plane where $\mu(Re, \tan(\Theta)) > 0$. The line $\mu(Re, \tan(\Theta)) = 0$ is the limit in this plane under which the flow is absolutely stable.

3.3 Euler-Lagrange equations

To the variational problem which defines μ corresponds a set of Euler-Lagrange equations. The quadratic form can be written $\mathcal{H}\{\overrightarrow{v}\} = \overrightarrow{v}.L\overrightarrow{v}$, L being a linear symmetric operator. This operator is thus diagonalizable in an orthonormal basis and has real eigenvalues. One can prove that the infimum in equation 7 is reached when $\overrightarrow{v}$ is an eigenvector of L for its lowest eigenvalue λ. The Euler-Lagrange equations for this problem are then the equations of the eigenvalue problem for the linear operator L. The divergence free constraint is introduced in $\mathcal{H}$ with a Lagrange multiplier as $p\overrightarrow{\nabla}.\overrightarrow{v}$ which turns into a pressure term in L after an integration by parts. The Euler-Lagrange equations are then :

$$\lambda\overrightarrow{v} = -\nu\Delta\overrightarrow{v} + \frac{1}{2}[(\overrightarrow{\nabla}\overrightarrow{V_l}).\overrightarrow{v} + \overrightarrow{v}.(\overrightarrow{\nabla}\overrightarrow{V_l})] + \overrightarrow{\nabla}(p) \tag{8}$$

together with the incompressibility constraint $\overrightarrow{\nabla}.\overrightarrow{v} = 0$.

Since this problem is linear and periodic in both θ and z one can decompose $\overrightarrow{v}$ into Fourier modes in these directions and look for the stability of each one of these modes independently. Let us write one of these modes:

$$\overrightarrow{v} = (u(r), v(r), w(r))_{\{r,\theta,z\}}e^{im\theta}e^{ikz}$$

Inserting this development in the Euler-Lagrange equations and developing $\overrightarrow{V_l}$ yields :

$$\begin{aligned}
(-\lambda + A(r) + \frac{\psi}{r^2})u + Z(r)v + p_r - \nu\frac{1}{r}(ru_r)_r &= 0 && (9)\\
Z^*(r)u + (-\lambda + A(r) - \frac{\psi}{r^2})v + \frac{im}{r}p - \nu\frac{1}{r}(rv_r)_r &= 0 && (10)\\
(-\lambda + A(r) - \frac{\nu}{r^2})w + ikp - \nu\frac{1}{r}(rw_r)_r &= 0 && (11)
\end{aligned}$$

where the two functions A and Z are :

$$\begin{aligned}
A(r) &= \nu\left(k^2 + \frac{m^2+1}{r^2}\right)\\
Z(r) &= \frac{1}{2}(r\Gamma_r) + 2im\frac{\nu}{r^2}
\end{aligned}$$

Z^* is the complex conjugate of Z, and we introduced the angular velocity of the laminar solution $\Gamma(r) = \frac{V(r)}{r}$. The last equation of the system is the incompressibility constraint :

$$\frac{1}{r}(ru)_r + im\frac{v}{r} + ikw = 0 \tag{12}$$

To determine wether the flow is energy stable or not, one should solve this system of equations together with the homogeneous boundary conditions on $\overrightarrow{v}$ to find the lowest eigenvalue λ. The flow is energy stable if $\lambda > 0$.

4 Bounds on the energy stability limit

Our strategy in this section is not to solve the variational problem explicitly, but to find some bounds on the location of the line $\mu(Re, \tan(\Theta)) = 0$ in the $(Re, \tan(\Theta))$ plane. Two different techniques are used :

- In paragraphs 4.1 and 4.2 we specify a mode for $\overrightarrow{v}$ and we study the energy stability limit of this particular mode. If any mode of perturbation can grow, then the flow is not energy stable. This means that the energy stability limit of one particular mode of perturbation is an upper bound on the energy stability limit of the flow for an arbitrary perturbation.

- In paragraph 4.3 we derive a lower bound on the quadratic form $\mathcal{H}$. As long as this lower bound remains positive, $\mathcal{H}$ is positive and the flow is energy stable. This gives a lower bound on the energy stability limit, and thus a rigorous sufficient condition for the flow to be absolutely stable.

4.1 Stability of the mode $m = 0$, $k = 0$

Let us study perturbations which are axisymmetric and translation invariant in the z direction. Such perturbations correspond to the mode $m = 0$ and $k = 0$. For this mode the mass conservation equation is simply :

$$(ru)_r = 0 \Rightarrow u = u(R_2)\frac{R_2}{r}$$

but since $\overrightarrow{v}$ satisfies the homogeneous boundary conditions, $u(R_2) = 0$ and $u = 0$. To find the marginal energy stability limit we impose $\lambda = 0$ in the Euler-Lagrange equations (remember that since $\mathcal{L}$ is a symmetric operator, its eigenvalues are real). The azimuthal component of these equations simplifies to :

$$\nu v_{rr} + \nu\frac{v_r}{r} + (\psi - \nu)\frac{v}{r^2} = 0 \qquad (13)$$

We can look for power law solutions of this equation in the form $v(r) = Ar^p$. This leads to a second order equation in p :

$$p^2 = 1 - \alpha$$

We are interested in the case $\alpha > 1$ which corresponds to the most unstable situation. We obtain two values of p and the corresponding solution v:

$$\begin{aligned} p &= \pm i\sqrt{\alpha - 1} \\ v(r) &= A\cos(\sqrt{\alpha-1}\ln(\frac{r}{R_2})) + B\sin(\sqrt{\alpha-1}\ln(\frac{r}{R_2})) \end{aligned}$$

The first boundary condition $v(R_2) = 0$ imposes $A = 0$ while the second one imposes :

$$v(R_1) = 0 = B\sin(\sqrt{\alpha-1}\ln(\eta)) \Rightarrow B = 0 \text{ or } \sqrt{\alpha-1}\ln(\eta) = q\pi, q \in \mathbb{Z}^*$$

The first mode to become non energy stable as α increases is the mode $q = 1$, and the corresponding critical value of α is :

$$\alpha_c = 1 + \frac{\pi^2}{(\ln(\eta))^2}$$

We come back to the $(Re, \tan(\Theta))$ plane using equation 4 to find our first upper bound on the energy dissipation limit :

$$Re_1(\tan(\Theta)) = \left(1 + \frac{\pi^2}{(\ln(\eta))^2}\right)\frac{1-\eta}{\tan(\Theta)} \qquad (14)$$

The line $Re_1(\tan(\Theta))$ has been drawn on figure 4 for several values of the geometrical factor η. This upper bound shows that whatever the injection angle is, energy stability is lost when the Reynolds number becomes high enough.

We can explain why the mode $(m = 0, k = 0)$ will grow for large values of α : a small perturbation $v_0 = v(t = 0)$ in the azimuthal velocity field at an initial radius $R_0 = R(t = 0)$ will be advected towards the center by the suction. If α is large enough, the flow is nearly inviscid and the fluid conserves its angular momentum during the inward motion. Hence the velocity perturbation becomes :

$$v(R(t), t) = v_0\frac{R_0}{R(t)}, \text{ with } R(t) \leq R_0$$

which means that the kinetic energy of this perturbation increases : the mode is not energy stable. However, when the perturbation is advected all the way to the boundary layer near R_1, the viscous effects dissipate the angular momentum of the perturbation and the perturbation is swept away by the suction. For this reason we expect to see transient growth for this mode more than an actual instability.

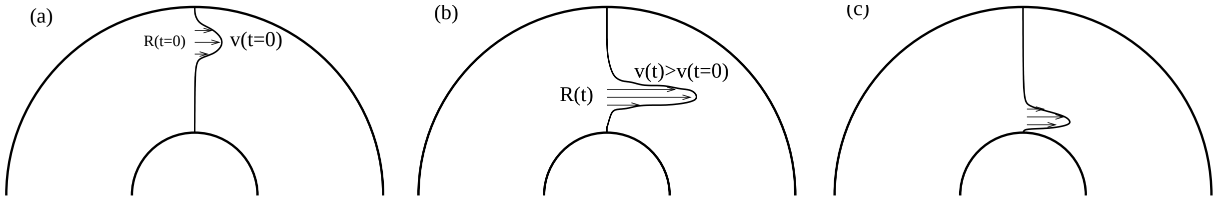

Figure 3: Expected behaviour of an energy unstable mode for $(m = 0, k = 0)$: a perturbation at $t = 0$ (a) is advected by the suction and speeds up (b). When it reaches the boundary layer the fluid loses its angular momentum and the perturbation is swept away (c).

4.2 Stability of a given velocity profile

Another method to get an upper bound on the energy stability limit is to specify completely the structure of a mode (i.e. specify m, k, $u(r)$, $v(r)$) and look for its energy stability limit. The quadratic form can be developed in cylindrical coordinates as :

$$\mathcal{H}\{\overrightarrow{v}\} = \int_\tau \left[\nu|\overrightarrow{\nabla}\overrightarrow{v}|^2 + (r\Gamma_r)uv - \frac{\psi}{r^2}(v^2 - u^2)\right] d\tau \tag{15}$$

The first term in this integral is the damping due to viscous dissipation. The second term is the only one which depends on the azimuthal velocity profile of the laminar solution. The last term is proportional to ψ and is responsible for the upper bound we found in the last paragraph (the azimuthal velocity profile of the laminar solution did not play any role in the derivation of this bound since there is no dependance in V in equation 13). In this paragraph we would like to study specifically the effect of the azimuthal velocity profile of the laminar solution on the energy stability of the flow. We thus choose :

$$u(r) = -v(r)$$

which causes the last term of $\mathcal{H}$ to vanish. As we are going to evaluate some quadratic quantities we do not want to use complex notations. Let us write :

$$\overrightarrow{v} = \left| \begin{array}{ll} -v & \cos(m\theta)\cos(kz) \\ v & \cos(m\theta)\cos(kz) \\ w & \cos(m\theta + \phi_\theta)\cos(kz + \phi_z) \end{array} \right.$$

This decomposition leads to :

$$\frac{1}{2\pi L_z}\int_{\theta=0}^{\theta=2\pi}\int_{z=0}^{z=L_z} |\overrightarrow{\nabla}\overrightarrow{v}|^2 d\theta dz = \frac{(v_r)^2}{2} + \frac{(w_r)^2}{4} + \left(k^2 + \frac{(m+1)^2}{r^2}\right)\frac{v^2}{2} + \left(k^2 + \frac{m^2}{2r^2}\right)\frac{w^2}{2} \tag{16}$$

and w can be computed in terms of v using the incompressibility constraint $\overrightarrow{\nabla}.\overrightarrow{v} = 0$:

$$-\frac{1}{r}(rv)_r\cos(m\theta)\cos(kz) - \frac{m}{r}v\sin(m\theta)\cos(kz) - kw\cos(m\theta + \phi_\theta)\sin(kz + \phi_z) = 0$$

Hence $\phi_z = \frac{\pi}{2}$, and :

$$w^2 = \frac{1}{k^2r^2}(r^2v_r^2 + 2rvv_r + (m^2+1)v)$$

Moreover we can notice that $(w_r)^2 = \frac{((w^2)_r)^2}{4w^2}$, with :

$$(w^2)_r = \frac{2}{k^2r^2}\left[-(m^2+1)\frac{v^2}{r} + r(v_r)^2 + m^2vv_r + rvv_{rr} + r^2v_rv_{rr}\right]$$

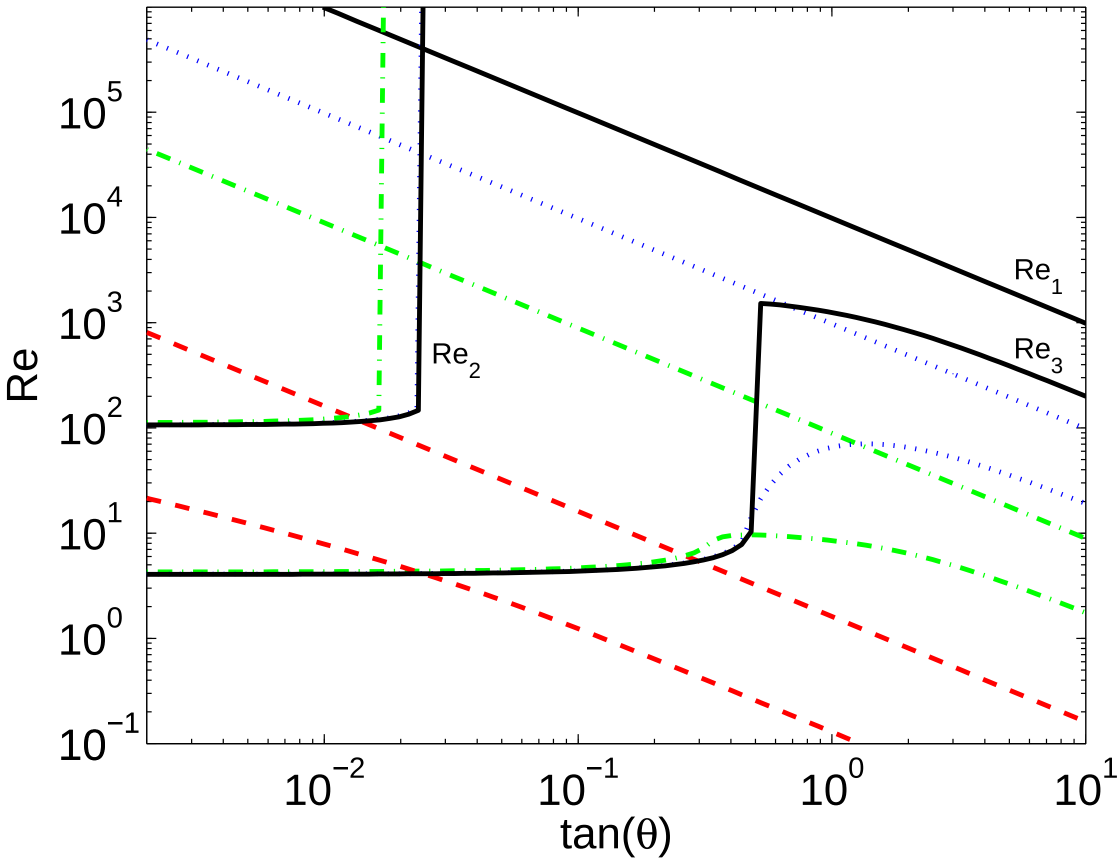

Figure 4: The three bounds on the energy stability limit. Re_1 is a straight line which decreases like $\tan(\Theta)^{-1}$. The bound Re_2 is out of the picture for $\eta = 0.02$, and makes the right angle shape in the upper left corner for η close to 1. The lower bound Re_3 is the lowest curve for every value of η. (dashed line : $\eta = 0.02$, dash-dotted line : $\eta = 0.9$, dotted line : $\eta = 0.99$, solid line : $\eta = 0.999$)

The energy stability limit of this mode is reached when $\mathcal{H}\{\overrightarrow{v}\} = 0$. Using equation 16, this energy stability limit becomes :

$$\int_{r=R_1}^{r=R_2} \left[(v_r)^2 + \frac{(w_r)^2}{2} + (1+m)^2 \frac{v^2}{r^2} + \frac{m^2}{2}\frac{w^2}{r^2} + k^2 v^2 + k^2 \frac{w^2}{2} - \frac{Re}{1-\eta}\frac{r\Gamma_r}{2R_2^2\Omega} v^2 \right] r dr = 0$$

where every term can be expressed in terms of v, v_r and v_{rr}. We chose $v(r)$ to be the simplest velocity profile that satisfies the boundary conditions on both u and v (since $u = -v$) :

$$v(r) = A(r - R_1)^2 (r - R_2)^2$$

All the integrals in equation 17 can be computed and we are left with an implicit equation in Re, $\tan(\Theta)$ and η which can be solved numerically. The best upper bound that we find with this method is for $(k = \frac{\pi}{R_2 - R_1}, m = 0)$. This mode corresponds to the well-known Taylor vortices. It is interesting to see that although the flow without suction is a stable configuration of the Taylor-Couette flow, a little bit of suction allows Taylor vortices to grow (they will at least have a transcient growth). The corresponding upper bound on the energy stability limit is called $Re_2(\tan(\Theta))$ and has been drawn for several values of η on figure 4. This bound goes to infinity for a finite value of the injection angle Θ. Around this value of Θ the quantity Γ_r becomes negative in a large region of the gap, so that all the terms in equation 17 are positive and the equation does not admit a solution anymore.

4.3 Lower bound on the energy stability limit

Let us define :

$$\mathcal{F}\{\overrightarrow{v}\} = \int_\tau (r\Gamma_r)uv - \frac{\psi}{r^2}(v^2 - u^2)d\tau$$

To find a lower bound on $\mathcal{H}$ one has to consider the fact that $\overrightarrow{v}$ cannot be arbitrarily large and match the homogeneous boundary conditions without having large gradients too. We will thus try to find a lower bound on $\mathcal{F}$ (which can be negative!) in terms of $||\overrightarrow{\nabla}\overrightarrow{v}||^2$. First of all we can get rid of the positive term $\frac{\psi}{r^2}u^2$ in $\mathcal{F}$. Using the inequality $|uv| \leq \frac{1}{2}[\frac{1}{c}u^2 + cv^2]$ which is valid for any $c > 0$, we get:

$$\mathcal{F}\{\overrightarrow{v}\} \geq -\int_\tau \frac{|r\Gamma_r|}{2}\left(\frac{1}{c(r)}u^2 + c(r)v^2\right) + \frac{\psi}{r^2}v^2 d\tau = -\int_\tau u^2\left(\frac{|r\Gamma_r|}{2c}\right) + v^2\left(\frac{\psi}{r^2} + c\frac{|r\Gamma_r|}{2}\right)d\tau$$

$c(r)$ is chosen in such a way that the coefficients of u^2 and v^2 are equal :

$$\frac{|r\Gamma_r|}{2c} = \frac{\psi}{r^2} + c\frac{|r\Gamma_r|}{2} \Rightarrow c^2 + \frac{2\psi}{r^3|\Gamma_r|}c - 1 = 0$$

$$\Rightarrow \begin{cases} c(r) = \frac{\zeta}{2}\left(\sqrt{1+\frac{4}{\zeta^2}} - 1\right) \\ \text{with } \zeta = \frac{2\psi}{r^3|\Gamma_r|} \end{cases}$$

This choice of c leads to :

$$\mathcal{F}\{\overrightarrow{v}\} \geq -\int_\tau \frac{|r\Gamma_r|}{2c}(u^2+v^2)d\tau = -\int_\tau \frac{\psi}{2r^2}\left(\sqrt{1+\frac{4}{\zeta^2}} + 1\right)(u^2+v^2)d\tau \tag{17}$$

We now use the fundamental theorem of calculus and the Schwartz inequality to get :

$$|v(r)| = \left|\int_{R_1}^r \frac{1}{\sqrt{\tilde{r}}}\sqrt{\tilde{r}}v_r(\tilde{r})d\tilde{r}\right| \leq \sqrt{\int_{R_1}^r \frac{1}{\tilde{r}}d\tilde{r}}\sqrt{\int_{R_1}^r |v_r(\tilde{r})|^2\tilde{r}d\tilde{r}}$$

The same technique can be applied to u and yields :

$$\begin{cases} |u| \leq \sqrt{\ln\left(\frac{r}{R_1}\right)}\sqrt{\int_{R_1}^r |u_r(\tilde{r})|^2\,\tilde{r}d\tilde{r}} \\ |v| \leq \sqrt{\ln\left(\frac{r}{R_1}\right)}\sqrt{\int_{R_1}^r |v_r(\tilde{r})|^2\,\tilde{r}d\tilde{r}} \end{cases}$$

Finally :

$$u^2 + v^2 \leq \ln\left(\frac{r}{R_1}\right)\int_{R_1}^r \left(|u_r(\tilde{r})|^2 + |v_r(\tilde{r})|^2\right)\tilde{r}d\tilde{r} \tag{18}$$

If we use this inequality in 17 the integrals separate and we find :

$$\mathcal{F}\{\overrightarrow{v}\} \geq -\int_{R_1}^{R_2} \frac{\psi}{2r}\ln\left(\frac{\tilde{r}}{R_1}\right)\left(\sqrt{1+\frac{4}{\zeta^2}} + 1\right)d\tilde{r}\int_\theta\int_z\int_{R_1}^r \left(|u_r(\tilde{r})|^2 + |v_r(\tilde{r})|^2\right)\tilde{r}d\tilde{r}d\theta dz$$

hence :

$$\mathcal{F}\{\overrightarrow{v}\} \geq -\int_{R_1}^{R_2} \frac{\psi}{2r}\ln\left(\frac{\tilde{r}}{R_1}\right)\left(\sqrt{1+\frac{4}{\zeta^2}} + 1\right)d\tilde{r}\quad ||\overrightarrow{\nabla}\overrightarrow{v}||^2$$

The lower bound on $\mathcal{H}$ is finally :

$$\mathcal{H}\{\overrightarrow{v}\} = \nu||\overrightarrow{\nabla}\overrightarrow{v}||^2 + \mathcal{F}\{\overrightarrow{v}\} \geq \left[\nu - \int_{R_1}^{R_2} \frac{\psi}{2r}\ln\left(\frac{\tilde{r}}{R_1}\right)\left(\sqrt{1+\frac{4}{\zeta^2}} + 1\right)d\tilde{r}\right]\quad ||\overrightarrow{\nabla}\overrightarrow{v}||^2$$

So that $\mathcal{H}$ is necessarily positive if :

$$\nu - \int_{R_1}^{R_2} \frac{\psi}{2r} \ln\left(\frac{\tilde{r}}{R_1}\right) \left(\sqrt{1+\frac{4}{\zeta^2}}+1\right) d\tilde{r} \geq 0$$

If we define $r = R_2 x$ and compute $\zeta(x)$ for the laminar azimuthal velocity profile found in section 2.3, the lower bound on the energy stability limit becomes :

$$\frac{\alpha}{2} \int_{\eta}^{1} \frac{\ln\left(\frac{x}{\eta}\right)}{x} \left(\sqrt{1+\frac{4}{\zeta^2}}+1\right) dx = 1 \tag{19}$$

$$\text{with } \zeta(x) = 2\tan\Theta \frac{|\eta^{2+\alpha}-1|}{|\alpha x^{2+\alpha}+2\eta^{2+\alpha}|} \tag{20}$$

To this lower bound corresponds a line $Re_3(\tan(\Theta))$ which has been drawn for several values of η on figure 4. Under this line the flow is absolutely stable.

5 Numerical computation of the energy stability limit

In a study on the plane Couette flow with suction, Doering Spiegel and Worthing [1] found that the flow was absolutely stable if the injection angle was above a critical value $\Theta_c \simeq 3^o$. At this value of the entry angle the energy stability limit goes to infinity. In the cylindrical problem, the upper bound found in 4.1 clearly discards the possibility of such a behaviour. One may wonder how the shape of the energy stability limit will evolve from the plane Couette limit ($\eta \to 1$) to a cylindrical geometry. To answer this question, we solved numerically the eigenvalue problem in 3.3 to compute the actual energy stability limit.

5.1 Simplification of the system of equations

As a first step we can reduce as much as possible the number of variables and equations in the system. Taking the divergence of the vectorial form of the Euler-Lagrange equation and using the incompressibility constraint we get :

$$\Delta p = -\frac{1}{2r}(r^2\Gamma_r v)_r - \frac{im}{2r}(r\Gamma_r)u + \frac{\psi}{r^2}\left[-u_r + \frac{u}{r} + \frac{imv}{r}\right] \tag{21}$$

We can apply the operator Δ to equation 9 and use the relation :

$$\Delta(p_r) = (\Delta p)_r + \frac{p_r}{r^2} - \frac{2m^2}{r^3}p$$

to remove $\Delta(p_r)$. the remaining terms in p are $(\Delta p)_r$, p_r and p. They can be expressed in terms of u, v and their derivatives using equations 21, 9 and 10. This leads to the first differential equation of a system of two equations in u and v :

$$\begin{aligned}
&\lambda\left[\frac{-2im}{r^2}v + u_{rr} + \frac{1}{r}u_r - (k^2+\frac{m^2+1}{r^2})u\right] = (-\nu)\,u_{rrrr} + \left(-\frac{2\nu}{r}\right)u_{rrr} + \left(2A+\frac{\nu}{r^2}\right)u_{rr} \\
&+\left(\frac{2A}{r} - \frac{\nu}{r^3} + 2A_r - \frac{im\Gamma_r}{2}\right)u_r + \left(A_{rr} + \frac{A_r}{r} - A(k^2+\frac{m^2+1}{r^2}) - \frac{im\Gamma_{rr}}{2} - \frac{2im}{r^2}Z^*\right)u + \left(\frac{4im\nu}{r^2}\right)v_{rr} \\
&+\left(-\frac{4im\nu}{r^3}\right)v_r + \left(\frac{6im\nu}{r^4} - Z(k^2+\frac{m^2}{r^2}) - \frac{2imA}{r^2}\right)v + \psi\left[-\left(\frac{k^2}{r^2}+\frac{m^2}{r^4}\right)u + \frac{im}{r^3}v_r - \frac{im}{r^4}v\right]
\end{aligned} \tag{22}$$

To get the second equation of the system w is expressed in terms of u and v using the mass conservation equation 12. Inserting w in equation 11 we get p, which can be replaced in equation 10. This leads to the equation :

$$\lambda\left[-\frac{im}{r}u_r-\frac{im}{r^2}u+(k^2+\frac{m^2}{r^2})v\right]=\left(\frac{im\nu}{r}\right)u_{rrr}+\left(\frac{2im\nu}{r^2}\right)u_{rr}+\left(-\frac{im}{r}A\right)u_r \tag{23}$$
$$+\left(k^2Z^*-\frac{im}{r^2}A+\frac{2im\nu}{r^4}\right)u+\left(-\nu(k^2+\frac{m^2}{r^2})\right)v_{rr}+\left(\frac{\nu}{r}(-k^2+\frac{m^2}{r^2})\right)v_r$$
$$+\left(A(k^2+\frac{m^2}{r^2})-\frac{2\nu m^2}{r^4}+\frac{k^2\psi}{r^2}\right)v$$

This system has derivatives up to the fourth order in u and to the second order in v. We have four boundary conditions on u and two on v, which is enough to solve it.

5.2 Numerical resolution of the eigenvalue problem

The system of equation was solved using a finite-difference method. If N is the resolution, the functions u and v are discretized on the domain $[R_1, R_2]$ as :

$$u=(u_1,u_2,...,u_{N-1})$$
$$v=(v_1,v_2,...,v_{N-1})$$

with $u_n = u(r = R_1 + nh)$ and $h = \frac{R_2-R_1}{N}$. The eigenvalue problem is then replaced by a difference equation using the central difference approximations to the derivatives. Each derivative can be written as a matrix which coefficients can be determined from the four following Taylor developments :

$$f(x\pm h)=f(x)\pm hf^{(1)}(x)+\frac{h^2}{2}f^{(2)}(x)\pm\frac{h^3}{6}f^{(3)}(x)+\frac{h^4}{24}f^{(4)}(x)+O(h^5)$$
$$f(x\pm 2h)=f(x)\pm 2hf^{(1)}(x)+2h^2f^{(2)}(x)\pm\frac{4}{3}h^3f^{(3)}(x)+\frac{2}{3}h^4f^{(4)}(x)+O(h^5)$$

We get the approximations of the derivatives making linear combinations of these four equalities. For instance, we get for the first derivative :

$$f'(R_1+nh)=\frac{f(R_1+(n+1)h)-f(R_1+(n-1)h)}{2h}\ \text{if}\ 2\le n\le N-2$$
$$f'(R_1+h)=\frac{f(R_1+2h)-f(R_1))}{2h}=\frac{f(R_1+2h)}{2h}$$
$$f'(R_1+(N-1)h)=\frac{f(R_2)-f(R_1+(N-2)h)}{2h}=-\frac{f(R_1+(N-2)h)}{2h}$$

We used the boundary conditions to determine the extreme coefficients of the matrix. The computation of the matrices of the third and fourth order derivatives requires the use of 'ghost values' which are values of the functions on points out of the domain, such as $f(R_1-h)$ or $f(R_2+h)$. These quantities can be expressed in terms of values of the function inside the domain using the boundary conditions on the derivatives of f. For instance :

$$f'(R_1)=0=\frac{f(R1+h)-f(R_1-h)}{2h}\Rightarrow f(R_1-h)=f(R_1+h)$$

The matrices of the derivatives are tridiagonal and pentadiagonal :

$$D_r = \frac{1}{2h}\begin{pmatrix} 0 & 1 & & 0 \\ -1 & \ddots & \ddots & \\ & \ddots & \ddots & 1 \\ 0 & & -1 & 0 \end{pmatrix} \qquad D_{rr} = \frac{1}{h^2}\begin{pmatrix} -2 & 1 & & 0 \\ 1 & \ddots & \ddots & \\ & \ddots & \ddots & 1 \\ 0 & & 1 & -2 \end{pmatrix}$$

$$D_{rrr} = \frac{1}{2h^3}\begin{pmatrix} -1 & -2 & 1 & & 0 \\ 2 & 0 & \ddots & \ddots & \\ -1 & \ddots & \ddots & \ddots & 1 \\ & \ddots & \ddots & 0 & -2 \\ 0 & & -1 & 2 & 1 \end{pmatrix} \qquad D_{rrrr} = \frac{1}{h^4}\begin{pmatrix} 7 & -4 & 1 & & 0 \\ -4 & 6 & \ddots & \ddots & \\ 1 & \ddots & \ddots & \ddots & 1 \\ & \ddots & \ddots & 6 & -4 \\ 0 & & 1 & -4 & 7 \end{pmatrix}$$

Each equation of the system can be written as a linear combination of these matrices applied to u or v. The whole system can finally be written :

$$MX = \lambda NX$$

where $X = (u_1, \ldots, u_N, v_1, \ldots, v_N)$ and M and N are two 2x2 block matrices corresponding to the two sides of the equations. Each block represents the operator acting on one of the functions (u or v) in one of the two equations.

The eigenvalue problem $MX = \lambda NX$ can then be solved with the software MATLAB.

5.3 From plane Couette to cylindrical Couette

The energy stability limit has been drawn for several values of η on figure 5.3. When η is close to one and for very small values of the entry angle the energy stability limit remains constant at $Re \simeq 82$. This is the energy stability limit of the plane Couette flow. When $\theta \simeq 3^o$ the energy stability limit increases tremendously (several orders of magnitude), but cannot go to infinity as in the plane geometry. The cylindrical geometry allows some modes to grow. When $\tan(\Theta) \simeq 0.3$ the most unstable mode is $(m = 0, k = 0)$ and the energy stability limit coincides with the upper bound Re_1.

When η goes to zero, the behavior of the energy stability limit is totally different from the plane geometry. This limit corresponds to the situation where the outer radius goes to infinity while the inner radius is kept constant. The energy stability limit is then a monotonically decreasing function of the injection angle. The initial Reynolds number $Re(\Theta = 0)$ is higher in this case because we have chosen a definition of the Reynolds number based on the width of the gap. This definition is not relevant anymore when $\eta \to 0$ and should be replaced by $Re' = \frac{R_1^2\Omega}{\nu} = \frac{\eta^2}{1-\eta}Re$ since R_2 goes to infinity.

6 Bounds on the energy dissipation

The first bounds on turbulent quantities were introduced by Howard [2] to shed some light on Malkus assumption that turbulent convection would maximize the heat flux in turbulent convection [8]. Since then some related techniques have been developed such as the background method [6] [7]. Although the background method can be applied to any kind of geometry, people have mostly concentrated on shear layers and plane flows. Constantin [10] used the method to compute a bound on the energy dissipation for the Taylor-Couette flow without suction and Doering, Spiegel and Worthing successfully found a bound on the energy dissipation in a shear layer with suction. However, in the Taylor Couette problem with suction it appears a lot more challenging to find a bound, and we will show in this section that the background method in its usual formulation cannot be used.

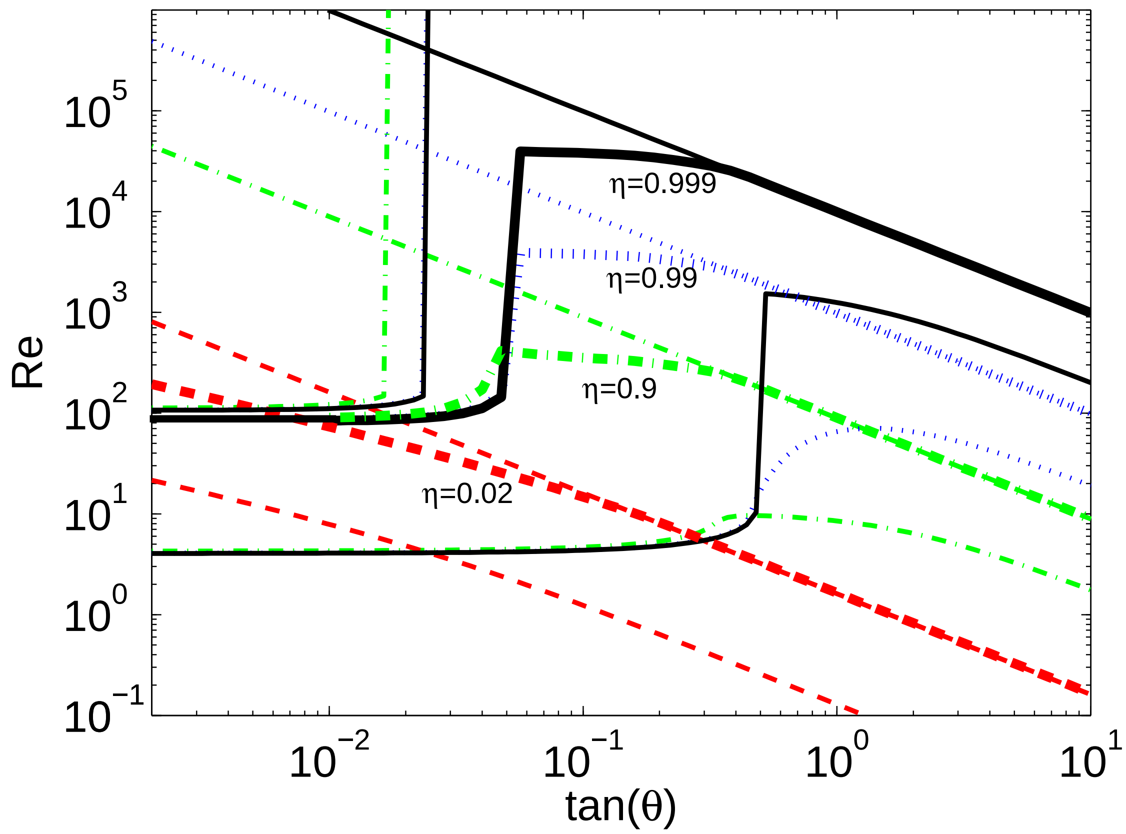

Figure 5: Energy stability limit of the Taylor-Couette flow with suction for different values of η.

6.1 The background method

The method uses a decomposition of the velocity field into a steady velocity profile and a time-dependant fluctuation field as in 3.1. The difference with the energy stability analysis is that the background profile remains to be chosen and is not necessarily the laminar solution. We can perform an integration by parts to write :

$$\int_\tau \vec{v}.\Delta\vec{V}d\tau = -\int_\tau (\vec{\nabla}\vec{V}).(\vec{\nabla}\vec{v})d\tau = -\frac{1}{2}\int_\tau |\vec{\nabla}\vec{u}|^2 - |\vec{\nabla}\vec{V}|^2 - |\vec{\nabla}\vec{v}|^2 d\tau$$

where the last equality comes from:

$$|\vec{\nabla}\vec{u}|^2 = |\vec{\nabla}\vec{V}|^2 + |\vec{\nabla}\vec{v}|^2 + 2(\vec{\nabla}\vec{v}).(\vec{\nabla}\vec{V})$$

Equation 6 can then be written as :

$$d_t\left(\frac{||\vec{v}||^2}{2}\right) + \frac{\nu}{2}||\vec{\nabla}\vec{u}||^2 = \frac{\nu}{2}||\vec{\nabla}\vec{V}||^2 - I \qquad (24)$$

$$\text{with } I = \int_\tau \frac{\nu}{2}|\vec{\nabla}\vec{v}|^2 + \vec{v}.(\vec{\nabla}\vec{V}).\vec{v} + \vec{v}.((\vec{V}.\vec{\nabla})\vec{V})d\tau \qquad (25)$$

The last term in I is linear in $\vec{v}$ which is not desirable in this procedure. To cancel this term we introduce another decomposition :

$$\vec{v} = \vec{W}(\vec{r}) + \vec{w}(\vec{r}, t)$$

where $\overrightarrow{W}$ and $\overrightarrow{w}$ are both divergence-free and verify the homogeneous boundary conditions. $\overrightarrow{W}$ is a steady flow whereas $\overrightarrow{w}$ is time dependant. This decomposition is inserted in I to find :

$$I = \mathcal{I}\{\overrightarrow{w}\} + \frac{\nu}{2}||\overrightarrow{\nabla}\overrightarrow{W}||^2 + \int_\tau \overrightarrow{W}.(\overrightarrow{\nabla}\overrightarrow{V}).\overrightarrow{W} + \overrightarrow{W}.((\overrightarrow{V}.\overrightarrow{\nabla})\overrightarrow{V})d\tau + \mathcal{L}\{\overrightarrow{w}\}$$

where :

$$\begin{aligned}
\mathcal{I}\{\overrightarrow{w}\} &= \int_\tau \frac{\nu}{2}|\overrightarrow{\nabla}\overrightarrow{w}|^2 + \overrightarrow{w}.(\overrightarrow{\nabla}\overrightarrow{V}).\overrightarrow{w}\,d\tau \\
\mathcal{L}\{\overrightarrow{w}\} &= \int_\tau \overrightarrow{w}.\left[-\nu\Delta\overrightarrow{W} + (\overrightarrow{\nabla}\overrightarrow{V}).\overrightarrow{W} + (\overrightarrow{W}.\overrightarrow{\nabla})\overrightarrow{V} + (\overrightarrow{V}.\overrightarrow{\nabla})\overrightarrow{V}\right]d\tau
\end{aligned}$$

$\overrightarrow{W}$ is then chosen to cancel the linear term in $\overrightarrow{w}$, that is $\mathcal{L}\{\overrightarrow{w}\} = 0$ for any vector field $\overrightarrow{w}$ that is divergence-free and satisfies the homogeneous boundary conditions (this does not necessarily imply that the bracket inside $\mathcal{L}$ has to be zero). If such a vector field $\overrightarrow{W}$ is chosen, it verifies $\mathcal{L}\{\overrightarrow{W}\} = 0$ which leads to:

$$\mathcal{I}\{\overrightarrow{W}\} = -\frac{1}{2}\int_\tau \overrightarrow{W}.((\overrightarrow{V}.\overrightarrow{\nabla})\overrightarrow{V})d\tau$$

The quantity I then becomes :

$$I = \mathcal{I}\{\overrightarrow{w}\} + \frac{1}{2}\int_\tau \overrightarrow{W}.((\overrightarrow{V}.\overrightarrow{\nabla})\overrightarrow{V})d\tau$$

This can be inserted in equation 24 to give :

$$d_t(||\overrightarrow{v}||^2) + \nu||\overrightarrow{\nabla}\overrightarrow{u}||^2 = \nu||\overrightarrow{\nabla}\overrightarrow{V}||^2 - \int_\tau \overrightarrow{W}.((\overrightarrow{V}.\overrightarrow{\nabla})\overrightarrow{V})d\tau - 2\mathcal{I}\{\overrightarrow{w}\}$$

where $\mathcal{I}\{\overrightarrow{w}\}$ is a quadratic form in $\overrightarrow{w}$. It is the same quadratic form as for the energy stability analysis with ν replaced by $\frac{\nu}{2}$. If we average this equation over a long time the left hand side becomes the average energy dissipation rate per unit mass (the time derivative averages to zero).

Here is the essence of the bounding procedure : If the background velocity profile is chosen so that $\mathcal{I}$ is a positive quadratic form, then this quadratic form can be dropped, which leads to the inequality :

$$\nu\overline{||\overrightarrow{\nabla}\overrightarrow{u}||^2} \leq \nu||\overrightarrow{\nabla}\overrightarrow{V}||^2 - \int_\tau \overrightarrow{W}.((\overrightarrow{V}.\overrightarrow{\nabla})\overrightarrow{V})d\tau$$

where the overline represents a long time average.

Usually the background profile is assumed to depend on the same coordinates as the laminar solution, and to verify the symmetries of the problem. For instance in a shear layer, the background is chosen as a function of the depth only. It seems natural to choose it independent of the horizontal coordinates since there is an invariance to any translation in these directions. For a cylindrical Couette flow we have an invariance to any translation in the θ and z directions. We are then tempted to chose an azimuthal background velocity profile which depends on r only, as for the laminar solution. This is a successful strategy for the classical Taylor Couette problem.

However, here is the problem that arises for the Taylor-Couette flow with suction : we find an upper bound on the energy stability limit of the flow studying the mode $(m = 0, k = 0)$. The derivation of this upper bound does not involve the azimuthal velocity profile. This means that for any injection angle Θ, and for any Reynolds number greater than $2Re_1(\Theta, \eta)$, the quadratic form $\mathcal{I}$ will not be a positive quadratic form, whatever function of r is chosen to be the background velocity profile. Therefore we cannot produce a bound on the energy dissipation with a background velocity depending only on r.

In studies on convection or shear layers [6] [7], the background velocity profiles happen to be very close to the average velocity profile of the flows at high Reynolds numbers, exhibiting very thin boundary layers near the walls and uniform profiles in the interior of the flow. This reinforces the common belief that the symmetries of the problem which are lost at relatively high Reynolds numbers through instabilities are recovered on average at even higher Reynolds numbers. The fact that we cannot choose a background velocity profile for the Taylor-Couette flow with suction which verifies the symmetries of the problem may raise the question of whether or not these symmetries are recovered at any Reynolds number.

7 Linear stability analysis

To understand how the symmetries of the system may be broken, as well as to complete the picture from the energy stability analysis, we shall now study the linear stability of the system.

7.1 Non-axisymmetric disturbances

Min and Lueptow [9] studied the linear stability of Taylor-Couette flow with suction, but their analysis includes only axisymmetric disturbances. They found that an inward flow has always a stabilizing effect and increases the critical Taylor number at which Taylor vortices appear. In the situation we are studying the inner cylinder remains steady. Without suction this configuration corresponds to a stable distribution of angular momentum and the Rayleigh criteria ensures that the flow is stable to axisymmetric perturbations. Since an inward flow has a stabilizing effect on these perturbations, we expect the flow to be linearly stable to any axisymmetric perturbation at any Reynolds number and any value of the entry angle Θ. For this reason our linear stability analysis focuses on non-axisymmetric perturbations. Such a perturbation breaks the invariance to translations in the θ direction.

In most instability mechanisms, one symmetry of the initial problem is broken at the onset of the primary instability whereas the other ones are broken through secondary instabilities. Since in our problem the most unstable perturbation has to break the invariance to translations in the θ direction, we expect it not to break the invariance to translations in the z direction. The most unstable mode would then have $(m \neq 0, k = 0)$. These are the modes of perturbation that we consider in the following linear stability analysis.

7.2 Linearization of the equations

We use the decomposition $\overrightarrow{u} = \overrightarrow{V_l} + \overrightarrow{v}$ and write a mode of perturbation as:

$$\overrightarrow{v} = (u(r), v(r), w(r))_{\{r,\theta,z\}} e^{-\lambda t} e^{im\theta}$$

where λ is now a complex number. We can set $w = 0$ and remove the vertical component of the Navier-Stokes equation without loss of generality. The linearization of the two other components leads to :

$$-\nu u_{rr} - \frac{\psi + \nu}{r} u_r + A_1 u - \lambda u + Z_1 v + p_r = 0 \quad (26)$$

$$-\nu v_{rr} - \frac{\psi + \nu}{r} v_r + A_2 v - \lambda v + Z_2 u + \frac{imp}{r} = 0 \quad (27)$$

with :

$$\begin{aligned}
A_1 &= im\frac{V}{r} + \frac{\psi}{r^2} + \nu\frac{m^2+1}{r^2} \\
A_2 &= im\frac{V}{r} - \frac{\psi}{r^2} + \nu\frac{m^2+1}{r^2} \\
Z_1 &= \frac{2im\nu}{r^2} - \frac{2V}{r} \\
Z_2 &= V_r + \frac{V}{r} - \frac{2im\nu}{r^2}
\end{aligned}$$

The mass conservation equation becomes :

$$imv + (ru)_r = 0 \tag{28}$$

From equation 28 v can be expressed in terms of u. This expression of v is then inserted in equation 27 to get p in terms of u. p is differentiated with respect to r and injected into equation 26. This leads to a fourth order ODE in u :

$$\begin{aligned}
&\left[\nu r^2\right] u_{rrrr} + \left[(6\nu + \psi) r\right] u_{rrr} + \left[\nu(6 - m^2) + 3\psi - r^2 A_2\right] u_{rr} \\
&+ \left[-\frac{\psi + \nu}{r} m^2 + imrZ_1 + imrZ_2 - r^2 (A_2)_r - 3rA_2\right] u_r \\
&+ \left[m^2 A_1 + imZ_1 + imZ_2 + imr(Z_2)_r - r(A_2)_r - A_2\right] u = \lambda \left[-r^2 u_{rr} - 3ru_r + (m^2 - 1)u\right]
\end{aligned} \tag{29}$$

u and its first derivative must vanish at the 2 boundaries, which is enough boundary conditions to solve this equation.

7.3 Numerical computation of the linear stability limit

Equation 29 is an eigenvalue problem which can be solved numerically with the method described in 5.2. The linear stability limit is much higher than the energy stability limit in terms of Reynolds number and α. For this reason a very high resolution is needed to determine it. The finite resolution of the computation leads to a maximal value of α above which the linear stability limit cannot be easily determined.

The linear stability limit of different modes was represented on figures 6 and 7 for $\eta = 0.5$ and $\eta = 0.9$. The energy stability limit was added to the picture to make the comparison easier. There is a linear instability at small injection angles. The most unstable modes have $m \sim \frac{R_2}{R_2 - R_1} = \frac{1}{1-\eta}$, which corresponds to circular cells between the two cylinders.

At a certain value of the injection angle the linear stability limit seems to go to infinity. An analytical proof of this remains to be established. Comparing the limits obtained for the two values of η we see that the more cylindrical the geometry, the more linearly unstable the flow. From $\eta = 0.9$ to $\eta = 0.5$, the minimum value of the critical Reynolds number goes from approximately 10^4 to 2.10^3, and the maximum value of the injection angle that allows a linear instability increases by almost an order of magnitude. To emphasize the fact that this linear instability is found in the bulk of the flow (and not in the boundary layer as in the plane Couette flow with suction), a few pictures of the unstable mode at the onset of instability were added. For $\eta = 0.9$, the mode consists in only one row of rotating cells in the width of the gap if the injection angle is small. When the injection angle is closer to its critical value, this row splits into two rows of counter-rotating cells. For $\eta = 0.5$, we observe that the cells are closer to the outer boundary (the injection boundary) when the injection angle is far from the most unstable injection angle. At the most unstable value of the injection angle the cells occupy the whole width of the gap.

One should notice that in the limit of no suction and rotation only ($\tan(\Theta) \to 0$), the linear stability limit goes to infinity and the flow is stable. On the other hand, if there is only suction and no rotation ($Re \to 0, \alpha \to \infty$), we lose the instability too. This means that the linear instability exists only when both rotation and accretion are taken into account. It is lost if only one of these two ingredients is considered.

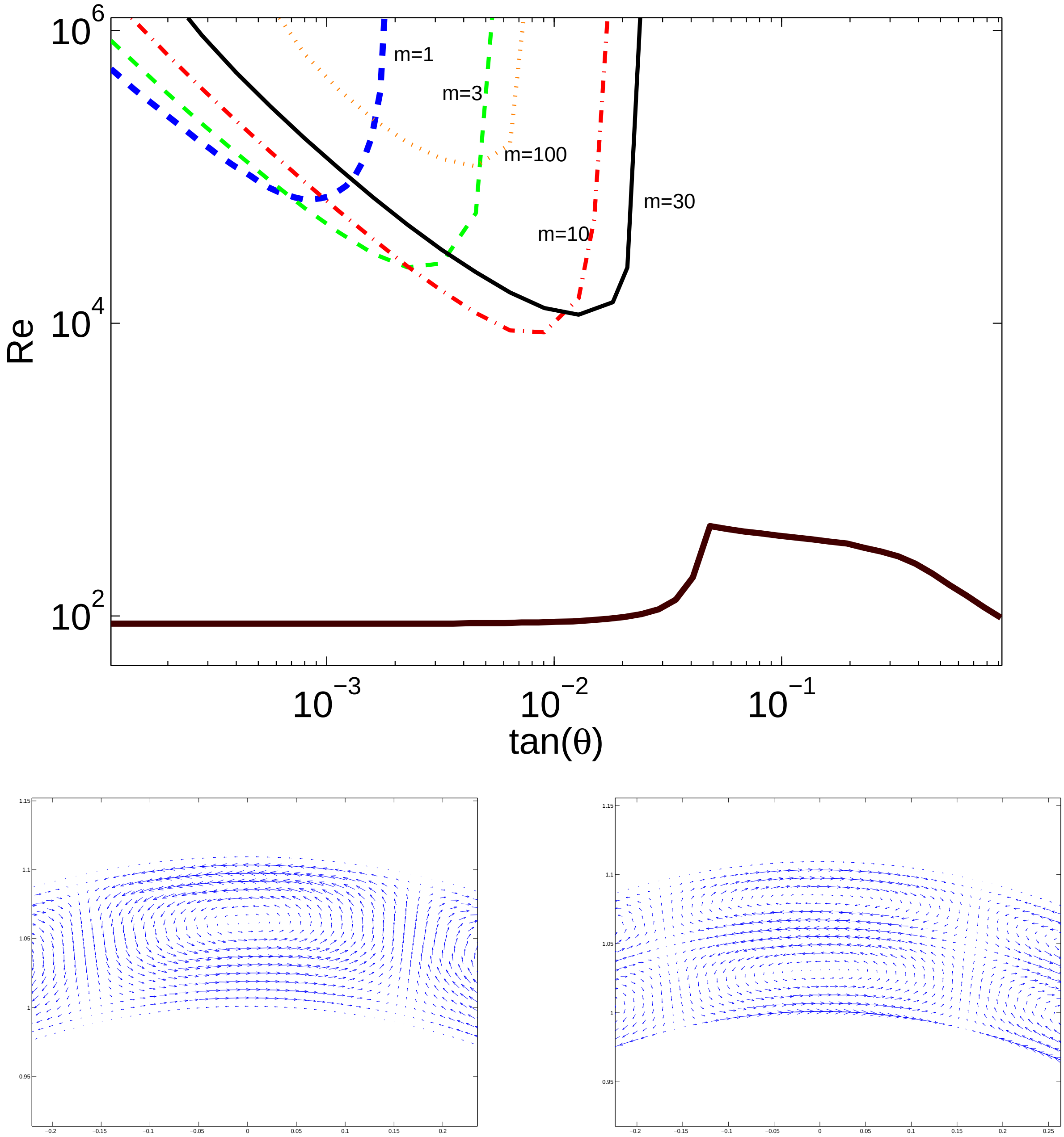

Figure 6: **Upper picture :** Linear stability limit of several modes for $\eta = 0.9$ (thick dashed line : $m = 1$, dashed line : $m = 3$, dash-dotted line : $m = 10$, solid line : $m = 30$, dotted line : $m = 100$). The energy stability limit has been added to make the comparison easier (thick solid line). **Lower left :** Unstable mode at the onset of instability for $m = 10$, $\tan(\Theta) = 0.003$, $\eta = 0.9$. One row of rotating cells can be seen in the width of the gap. **Lower right :** Unstable mode at the onset of instability for $m = 10$, $\tan(\Theta) = 0.01$, $\eta = 0.9$. Two rows of counter-rotating cells can be seen in the width of the gap.

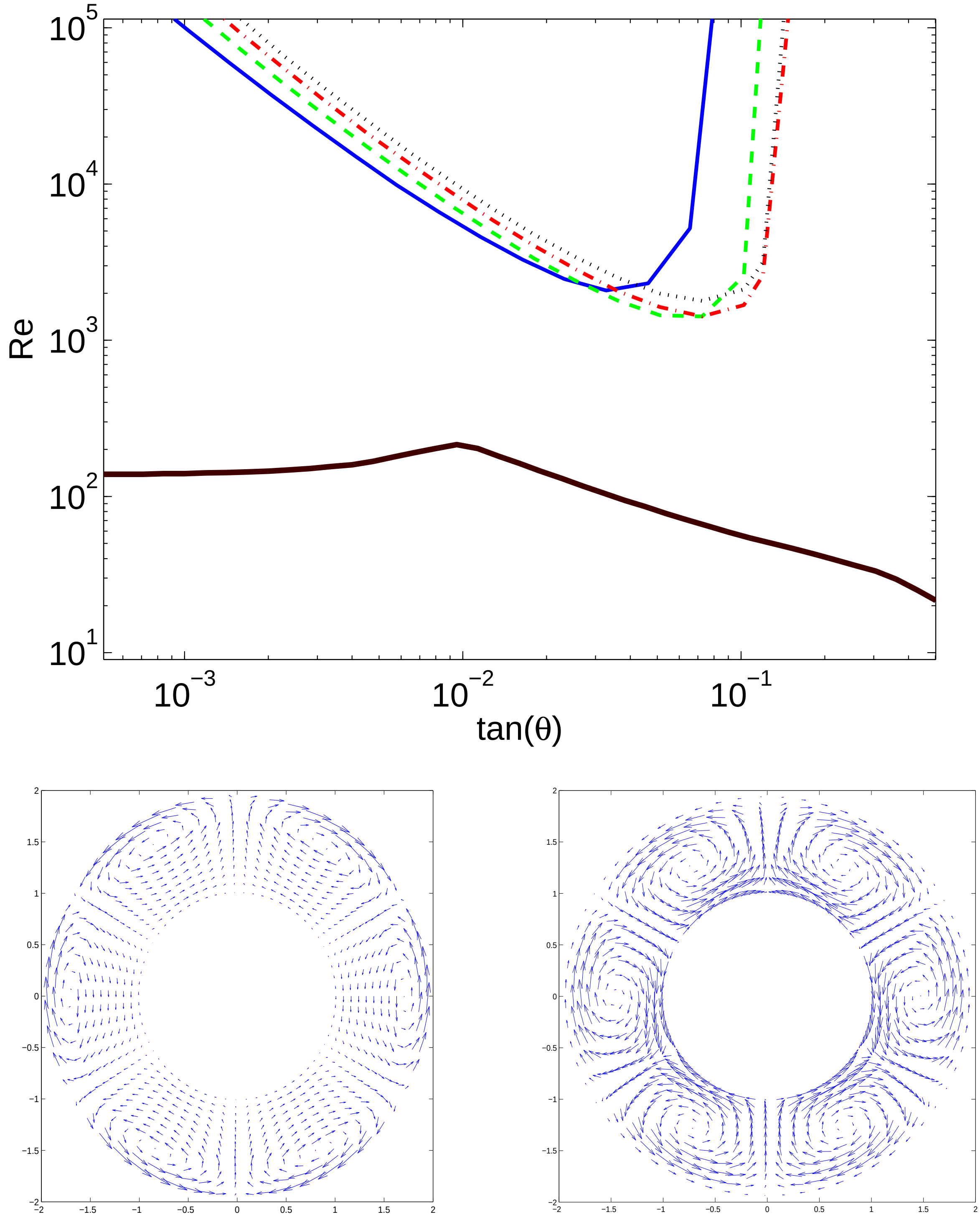

Figure 7: **Upper picture :** Linear stability limit of several modes for $\eta = 0.5$. In this more cylindrical geometry, linear instability is found for lower values of the Reynolds number and up to higher values of the injection angle. (solid line : $m = 1$, dashed line : $m = 2$, dash-dotted line : $m = 3$, dotted line : $m = 4$, thick solid line : energy stability limit). **Lower left :** Unstable mode at the onset of instability for $m = 3$, $\tan(\Theta) = 0.008$, $\eta = 0.5$. The cells are close to the injection boundary. **Lower right :** Unstable mode at the onset of instability for $m = 3$, $\tan(\Theta) = 0.08$, $\eta = 0.5$. The cells are in the whole width of the gap.

8 Conclusion

The actual energy stability limit has been computed for different configurations of the Taylor-Couette flow with suction : this flow is not energy stable provided that the Reynolds number is high enough, and we cannot rule out the possibility of a non-linear instability in such a flow. Moreover, this flow can be linearly unstable for certain values of the parameters : the combined efffects of rotation and accretion lead to a new linear instability which does not exist if only one of these ingredients is present.

This could lead to a scenario for a non-linear instability in an accretion disk : Let us consider a rotating disk without accretion. This disk is linearly stable but not energy stable. If it is subject to a perturbation, this perturbation could grow and carry out a little bit of angular momentum. This would drive accretion. Now that both rotation and accretion are present, the flow may not be linearly stable anymore and could become turbulent.

However, the flow we studied is very far from being a good model of an accretion disk and further work remains to be done to see if the results derived here could be applied to an actual accretion disk.

9 Acknowledgements

I would like to thank my supervisors C.Doering and E.Spiegel for their help during this summer. Thank you to all the GFD staff which gave me the great opportunity to come to the GFD program.

References

[1] C.R. Doering, E.A. Spiegel, R.A. Wothing *Energy dissipation in a shear layer with suction.* Physics of Fluids, 2000, volume 12, number 8.

[2] L.N. Howard. *Heat transport by turbulent convection.* Journal of Fluids Mechanics **17**, 405, (1963).

[3] S.A. Balbus, J.F. Hawley. *Instability, turbulence, and enhanced transport in accretion disks.* Review of modern physics volume 70, number 1 (1998).

[4] P. Drazin, W. Reid. *Hydrodynamic stability.* Cambridge University Press (1981)

[5] H.Ji, M.Burin, E.Schartman, J.Goodman. *Hydrodynamic turbulence cannot transport angular momentum effectively in astrophysical disks.* Nature, Volume 444 (2006)

[6] C.Doering, P.Constantin. *Variational bounds on energy dissipation in incompressible flows : III. Convection.* Phys. Rev. E **53**, 5957 (1996)

[7] C.Doering, P.Constantin. *Variational bounds on energy dissipation in incompressible flows : Shear flow.* Phys. Rev. E **49**, 4087 (1994)

[8] W.V.R. Malkus. *The heat transport and spectrum of thermal turbulence.* Proc. R. Soc. London, Ser. A **225**, 196 (1954).

[9] K. Min, R.M. Lueptow. *Hydrodynamic stability of viscous flow between rotating porous cylinders with radial flow.* Physics of Fluids, **6** (1) 1994.

[10] P. Constantin. *Geometric statistics in turbulence.* SIAM Review, Vol 36, No 1.